PROCEEDINGS A

royalsocietypublishing.org/journal/rspa

Research

Cite this article: Nezhad Hajian D, Parastesh F, Rajagopal K, Jafari S, Perc M, Klemenčič E. 2023 Chirality and curvature determine the meandering of spirals in multilayer excitable media. *Proc. R. Soc. A* **479**: 20230730. https://doi.org/10.1098/rspa.2023.0730

Received: 3 October 2023
Accepted: 24 November 2023

Subject Areas:
complexity

Keywords:
multilayer network, complex system, excitable media, pattern formation, mathematical biology

Author for correspondence:
Matjaž Perc
e-mail: matjaz.perc@gmail.com

Chirality and curvature determine the meandering of spirals in multilayer excitable media

Dorsa Nezhad Hajian[1], Fatemeh Parastesh[3], Karthikeyan Rajagopal[3], Sajad Jafari[1,2], Matjaž Perc[4,5,6,7,8] and Eva Klemenčič[4,9]

[1]Department of Biomedical Engineering, and [2]Health Technology Research Institute, Amirkabir University of Technology (Tehran polytechnic), Tehran, Iran
[3]Centre for Nonlinear Systems, Chennai Institute of Technology, Chennai 600069, Tamil Nadu, India
[4]Faculty of Natural Sciences and Mathematics, University of Maribor, Koroška cesta 160, 2000 Maribor, Slovenia
[5]Department of Medical Research, China Medical University Hospital, China Medical University, Taichung 404332, Taiwan
[6]Alma Mater Europaea, Slovenska ulica 17, 2000 Maribor, Slovenia
[7]Complexity Science Hub Vienna, Josefstädterstraße 39, 1080 Vienna, Austria
[8]Department of Physics, Kyung Hee University, 26 Kyungheedae-ro, Dongdaemun-gu, Seoul, Republic of Korea
[9]Faculty of Energy Technology, University of Maribor, Hočevarjev trg 1, 8270 Krško, Slovenia

DNH, 0000-0002-1190-3614; SJ, 0000-0002-6845-7539; MP, 0000-0002-3087-541X

We study the emergence of meandering spiral waves in a multilayer structure where two spirals, originating independently, evolve in space–time. The FitzHugh-Nagumo model, enhanced with electromagnetic induction effects, defines the nodal dynamics. The layers are chemically coupled, and the drift of spirals is influenced by interlayer flux coupling. An external magnetic flux force is also necessary to destabilize and unpin spiral rotors. The effects of unique characteristics of spiral patterns, like chirality and tip curvature, are assessed. We find that spirals often drift within a bounded meandering area; however, determining the drift directions and overall

THE ROYAL SOCIETY PUBLISHING

meandering regions is complex. The forced spiral generally drifts a greater distance, except for identical co-rotating spirals, which drift synchronously. Spirals with opposite chirality exhibit asynchronous drift and wavefront asymmetry, even with identical tip curvature. Regardless of chirality, non-identical spirals are geometrically aligned and amplified before drifting. Stimulating the more loosely curved spiral ensures both spirals drift.

1. Introduction

In excitable media, complex spatio-temporal patterns frequently emerge [1,2], indicative of medium self-sustainability and self-organization [3,4]. Many of them exhibit chiral structures, such as spiral-shaped patterns [5] that can influence a range of dynamic behaviours, precisely the excitability level of the medium [6]. Regarding human physiology, spiral waves have been observed in various sites, including the retina's surface, the middle brain cortex and the heart muscle, triggering disorders such as migraines [7], epileptic seizures [8] and fatal cardiac arrhythmias [9], respectively. A body of the literature highlights the link between spiral waves in Ventricular tachycardia and fibrillation [10,11]. Hence, in the biological context, the formation of spiral waves is often a sign of dysfunction. Consequently, in computational studies, various techniques have been used to terminate wave reentry, either by eliminating the stable rotor [12,13] or by making the spiral seed non-stationary [14], driving the rotor out of the medium.

Exploring the complex aspects of spiral dynamics, the movement of its free end has been a topic of interest [15]. The spiral rotating tip, the rotor, is not spatially stationary and may unpin from the initial locus [16]. Spiral wave drift refers to the type of motion in which the genius rotation of the spiral wave tip along a circular trajectory is accompanied by the meandering of the spiral tip through the plane [17]. In other words, the spiral structure consistently undergoes a rotational and translational motion. The unpinning process might be followed by suppressing spiral patterns, a desirable objective in addressing cardiac arrhythmia [18]. Pumir and Krinsky revealed that applying an external electric field to the cardiac tissue serves as an excitation source and unpins the rotor [19]. Consequently, several other strategies have been developed, such as electric pulse [20,21], field pacing [22] and recently polarized electric fields [23,24]. Optogenetic manipulation in extended models with photosensitive ion channels [25,26] and feedback-controlled forcing of spiral waves are cutting-edge methods employed to destabilize rotating tips [27]. Given the spatial arrangement of the medium, obstacles of proper size can lead spiral seeds to drift away from the heterogeneous site [28,29]. Moreover, the focal activity or reentrant seeds of spiral waves are organized by sites known as singularities (PS). Considerable efforts have been undertaken to determine the position of PSs [30,31], given that the drift of spiral waves often originates from their motion [32].

In terms of structural realization, biological tissues are fundamentally organized as a laminar complex composed of excitable planar networks [33]. Therefore, the interaction of several spiral waves in a single spatial domain, whether in two dimensions [34–36] or a multilayer complex [37–39], has been a concern. The motivation to study interactive propagation waves stems from biologically plausible scenarios. One key example is the occurrence of cardiac arrhythmias, which can arise from the competition between two spontaneous pacemakers with differing frequencies. The sinoatrial node serves as the regular source of wave propagation, while an abnormal pacemaker can be situated in a ventricle. The waves these pacemakers differ in source location and frequency and emerge independently. Therefore, understanding the rhythms resulting from the interplay of multiple independent pacemaking sites within the intricacies of a nonlinear medium is crucial [40]. Furthermore, concerning patterns emerged by multiple excitation sites in the brain, as observed through multi-channel electroencephalograms, there's potential for identifying mental disorders. Such findings emphasize the informative role of spatial patterns in biological media [41].

Although the waves tend to propagate within planar arrays, the third dimension's influence cannot be ignored entirely. The question of spiral wave interactive drift arises by extending the

spatial analysis to three dimensions. The drift of coupled spirals, each existing in a separate plane, seems relevant. Each spiral locus might meander along the propagating wavefronts of its counterpart. To the authors' knowledge, few works exist on the spiral wave drift caused by interactive rotational motion. Nagy-Ungvarai *et al*. [15] consider a bilayer structure with two coupled spirals of identical frequencies. It is claimed that spirals might undergo parallel and circular drifts. Besides, the frequency of rotation, the chirality, or handedness, [26,42] and curvature [16,43] are critical aspects of a spiral pattern. Hence, one might speculate the given feature might also affect the spirals' interplay in a multilayer configuration.

The Fitzhugh-Nagumo (FHN) model is a simplified representation that properly outlines the time-dependent firing of an excitable nerve cell [44,45]. Moreover, FHN's excitable regime makes it a suitable choice for simulating travelling waves [46,47]. This study employs the improved FHN model proposed by Ma *et al*. [48], in which a magnetic flux variable is considered. Such realization contributes to reproducing the electrical characteristics of myocardial cells or neurons more reasonably [49,50]. Given the spatial unsteadiness of spiral rotors under an electric field, the present report employs an external magnetic flux to unpin spiral waves, as a recent study has highlighted the sensitivity of travelling spiral waves in a multi-layered structure to magnetic flux [51]. The media is arranged in a bilayer complex where local neural arrays exchange signals through chemical synapses. The corresponding nodes in each layer are coupled via a magnetic flux. Our objective is to assess whether the interplay between self-sustained travelling spirals in interconnected layers leads to the drifting of spiral rotors. This framework investigates the interaction between spirals with opposing or matching chirality, denoted as counter-rotating and co-rotating spirals. Additionally, we analyse a significant aspect of spiral formation—the curvature of the rotating tip—by considering scenarios of coupling identical and non-identical spirals.

The paper is organized as follows: §2 discusses the nodal dynamics, network arrangement, intra- and inter-layer coupling schemes, and numerical implementations. This section also specifies the requirements for forming spirals with distinct curvature and chirality. Section 3 presents results for four distinct scenarios related to the coupling of spirals in the bilayer structure, focusing on the meandering direction and drift of the spiral seeds. Finally, §4 concludes the paper.

2. Methods and models

In the present work, the temporal evolution of neuronal arrays in each layer is ruled by the three-variable FHN model, in which the effect of electromagnetic induction is realized. The magnetic flux modulates the trans-membrane potential kinetic through a flux-controlled memristor whose gain is tunable. The model is spatially realized in a bilayer structure. The intralayer synaptic connection is chemical, and two layers are coupled via linear field coupling. Therefore, the spatio-temporal description of the memristive FHN [48] bilayer structure is as follows:

$$\left.\begin{aligned}
\dot{u}_{(i,j,1)} &= -k u_{(i,j,1)}(u_{(i,j,1)}-a)(u_{(i,j,1)}-1) - u_{(i,j,1)}v_{(i,j,1)} + k_0\rho(\varphi_{(i,j,1)})u_{(i,j,1)} + I^{syn}_{(i,j,1)},\\
\dot{v}_{(i,j,1)} &= \left(\varepsilon + \frac{v_{(i,j,1)}\mu_1}{u_{(i,j,1)}+\mu_2}\right)[-v_{(i,j,1)} - k u_{(i,j,1)}(u_{(i,j,1)}-a-1)],\\
\dot{\varphi}_{(i,j,1)} &= k_1 u_{(i,j,1)} - k_2\varphi_{(i,j,1)} + \varphi_{ext} + D(\varphi_{(i,j,2)} - \varphi_{(i,j,1)}),\\
\dot{u}_{(i,j,2)} &= -k u_{(i,j,2)}(u_{(i,j,2)}-a)(u_{(i,j,2)}-1) - u_{(i,j,2)}v_{(i,j,2)} + k_0\rho(\varphi_{(i,j,2)})u_{(i,j,2)} + I^{syn}_{(i,j,2)},\\
\dot{v}_{(i,j,2)} &= \left(\varepsilon + \frac{v_{(i,j,2)}\mu_1}{u_{(i,j,2)}+\mu_2}\right)[-v_{(i,j,2)} - k u_{(i,j,2)}(u_{(i,j,2)}-a-1)],\\
\text{and}\quad \dot{\varphi}_{(i,j,2)} &= k_1 u_{(i,j,2)} - k_2\varphi_{(i,j,2)} + \varphi_{ext} + D(\varphi_{(i,j,1)} - \varphi_{(i,j,2)})
\end{aligned}\right\} \tag{2.1}$$

The subscripts $(i,j,1)$ and $(i,j,2)$ define the nodal index of each layer where $i,j \in [1,100]$. u is trans-membrane potential, v adjusts the slow current variability, and the third variable φ describes the magnetic flux. The neural excitability is tuned by k, ε, μ_1 and μ_2 parameters. In the literature, the parameter setting is often taken as $k=8$, $\varepsilon=0.008$, $a=0.15$, $\mu_1=0.2$ and $\mu_2=0.3$ [52]. Electromagnetic induction gains are defined through k_1 and k_2 parameters which are numerically selected as $k_1=0.2$ and $k_2=1$ [48]. The synaptic current of the intralayer chemical connection is considered in I^{syn}. Two independent layers are coupled by magnetic flux, for which a diffusive scheme is considered [53]. For independent layers to exchange flux signal at an appropriately high intensity, the electromagnetic field coupling strength is set to $D=15$. Given the purpose of this paper, φ_{ext} is chosen as a destabilizing source for stationary spiral tips. The proper numerical range of external forcing flux is given in the forthcoming sections.

The flux-controlled memristor $\rho(\varphi)$ applies the magnetic flux feedback on the membrane's potential. By Faraday's law of electromagnetic induction, the memristive feedback corresponds to an induced current within the physical context. The Faradic current is tunable by the parameter k_0. For the spiral rotors to be destabilized and unpinned, the Faradic gain is set to $k_0=3$. The nonlinear memductance function $\rho(\varphi)$ is described by

$$\rho(\varphi)=\frac{\mathrm{d}q(\varphi)}{\mathrm{d}\varphi}=\alpha+3\beta\varphi^2. \tag{2.2}$$

The appropriate parameter implementation of the memristive nonlinear circuit is as $\alpha=0.1$ and $\beta=0.2$.

The Internodal connections of each lattice are realized through chemical synapses. The radius of the connection is local and limited to each node's eight nearest neighbours. The synaptic connection between diagonal nodes is taken to be half times weaker than axial ones. Such factors will result in a fine geometrical spiral shape, owning smoothly curved wavefronts. Note that such coupling configuration guarantees spatial invariance or isotropy, ensuring that the values of coupling parameters are independent of nodal indices. Evidence points to the drift of spiral waves on anisotropic surfaces [54,55]. However, given the focus of this report—specifically, the drift of spirals resulting from interactions between laminar spiral waves with different curvature and chirality—we deliberately avoid any anisotropy that might serve as a secondary reason for the drift of spiral seeds. Equation (2.3) denotes the chemical synapse scheme [56].

$$\begin{aligned} I_{ij}^{syn} = &-g_c(u_{ij}-V_{\mathrm{rev}}) \\ &\times\Big[\Gamma(\lambda,\theta,u_{(i+1)j})+\Gamma(\lambda,\theta,u_{(i-1)j})+\Gamma(\lambda,\theta,u_{i(j+1)})+\Gamma(\lambda,\theta,u_{i(j-1)}) \\ &+\frac{1}{2}\times\{\Gamma(\lambda,\theta,u_{(i+1)(j+1)})+\Gamma(\lambda,\theta,u_{(i+1)(j-1)})+\Gamma(\lambda,\theta,u_{(i-1)(j+1)}) \\ &+\Gamma(\lambda,\theta,u_{(i-1)(j-1)})\}\Big], \end{aligned} \tag{2.3}$$

where g_c defines the intensity of synaptic connection and V_{rev} is reversal potential, denoting a voltage threshold at which the equilibrium between inward and outward currents is achieved. The firing response of each neighbouring synaptic terminal resembles a threshold-like sigmoid behaviour. The function $\Gamma(\lambda,\theta,u)$ realizes a sigmoid s-carved relation as

$$\Gamma(\lambda,\theta,u)=\frac{1}{1+\mathrm{e}^{-\lambda(u-\theta)}}, \tag{2.4}$$

where λ is the sigmoid slope, and θ determines the firing threshold defining the operating point at which neurons smoothly respond according to slope λ. The chemical coupling parameters are closely associated with the spiral free-end curvature and the speed at which the spiral's locus rotates. Throughout this paper, we fixed $g_c=0.02$, and $\lambda=15$. For the rest of the chemical coupling numerics, two sets of $(V_{\mathrm{rev}},\theta)_T=(2,0.25)$ and $(V_{\mathrm{rev}},\theta)_L=(1.6,0.2)$ are selected to form tightly and loosely curved spirals, respectively. The tip curve of the spiral wave impacts the subsequent

Table 1. Local initial condition setup for the birth of clockwise and counterclockwise spiral waves.

clockwise	
ensemble 1	ensemble 2
setup (1)	
$u_0(45:55, 50:100) = 0.7$	$u_0(45:55, 50:100) = 0$
$v_0(45:55, 50:100) = 0.2$	$v_0(45:55, 50:100) = 0.8$
$\varphi_0(45:55, 50:100) = 0.1$	$\varphi_0(45:55, 50:100) = 0.2$
counterclockwise	
ensemble 1	ensemble 2
setup (2)	
$u_0(45:55, 1:50) = 0.7$	$u_0(45:55, 1:50) = 0$
$v_0(45:55, 1:50) = 0.2$	$v_0(45:55, 1:50) = 0.8$
$\varphi_0(45:55, 1:50) = 0.1$	$\varphi_0(45:55, 1:50) = 0.2$

radius of the circular wavefronts and the distance of two wavefronts in the ongoing sequence of wave propagation. In the case of the tightly curved tip, the subsequent wavefront tends to propagate at lower distances compared to the loosely curved scenario. Note that due to the parametric implementation of $(V_{\text{rev}}, \theta)_L = (1.6, 0.2)$, loose spirals wavefronts are lower in voltage and thus can be stimulated by slightly higher values of φ_{ext} without being unstable.

Prior to the coupling implementation, the laminar spiral wave emerges from the interplay between depolarized and hyperpolarized sites, established through the initial condition setup. The entire lattice is initially in a state of rest by $u_0 = v_0 = \varphi_0 = 0$, while two ensembles of local arrays are set to different initial values, as provided in table 1. By reversing the spatial arrangement of these two groups, it is possible to create clockwise and counterclockwise chirality. Thus, two setups, each consisting of depolarized and repolarized ensembles, are taken to create clockwise and counterclockwise rotating spiral waves. The two-dimensional sheet of each layer consists of a grid of 100×100 FHN neurons with no-flux boundaries. Given the spatially open boundary, waves tend to exit the observable region as they drift outward unless the source of propagation, which in this work is a spiral locus, remains active within the lattice. Simulations are performed by the Euler forward algorithm with temporal discretization of $\mathrm{d}t = 0.01$.

Regarding the (V_{rev}, θ) sets and the initial condition setups, four configurations of spiral waves can be realized as depicted in figure 1*a–d*. The monolayer portraits represent the initial moments at which reentrant wavefronts are taking form. Figure 1 caption explicitly states each subplot (V_{rev}, θ) and initial condition setting.

In each layer of chemically coupled neurons, an independent spiral wave travels with a specified curvature and chirality. When two layers are coupled through their magnetic flux, the circular voltage wavefronts in one layer indirectly influence the other, giving the nodal dynamics of each layer the impression of a time-varying stimulation. The curvature of the spiral tip and the handedness of its rotation are two critical features that define the spatiotemporal dynamics of the travelling wavefront. Thus, examining two coupled layers with spirals varying in the features mentioned above is an intriguing subject. In line with our objectives, we have considered four scenarios, labelled alphabetically from (a) to (d):

(a) Coupling of spirals that co-rotate and have identical tip curvature.
(b) Coupling of spirals that counter-rotate but possess identical tip curvature.
(c) Coupling of spirals that co-rotate but possess non-identical tip curvature.
(d) Coupling of spirals that counter-rotate and have non-identical tip curvature.

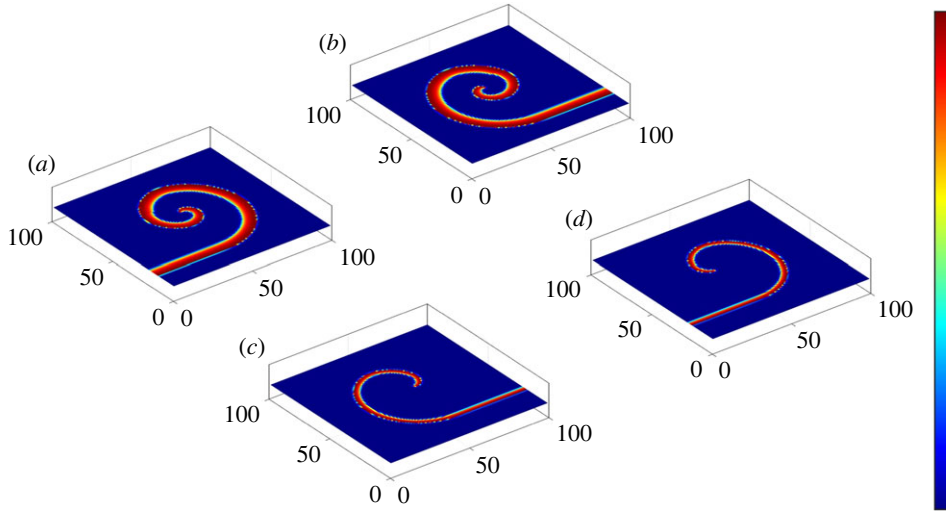

Figure 1. The four configurations of spiral waves realized in the present work: (*a*) tightly curved tip by $(V_{\text{rev}}, \theta)_T$ and counterclockwise by initial setup (2), (*b*): tightly curved tip $(V_{\text{rev}}, \theta)_T$ and clockwise by initial setup (1), (*c*): loosely curved by $(V_{\text{rev}}, \theta)_L$ and clockwise by initial setup (1), (*d*): loosely curved tip $(V_{\text{rev}}, \theta)_L$ and counterclockwise by initial setup (2). In figure 1*a*,*b*, the tip of the spiral revolves around a central locus at a relatively smaller distance from the centre compared to figure 1*c*,*d*. Consequently, the resultant wave curvature is tighter in cases 1(a) and 1(b).

In each case, the external magnetic flux φ_{ext} is applied to only one of the layers. We seek a proper magnitude of external flux that destabilizes the spiral core without causing any further breakup or elimination. Our experiments suggest that a large magnitude of φ_{ext} (specifically when $\varphi_{\text{ext}} > 0,58$) causes spiral waves to break up, and from the floating ends of these broken waves, multiple spiral seeds are born. Note that, in each layer, we aim to maintain the overall geometry of the single-core spiral, try to unpin it from the original node, cause it to drift, and ultimately track the meandering direction. Applying an overall magnetic flux of $\varphi_{\text{ext}} < 0,58$ to both layers preserves the geometry of the spiral wave. However, the drift caused by simultaneously stimulating both layers is not notable. Thus, in each case of study, we have only simulated one layer with an external flux in the range of $0.52 \leq \varphi_{\text{ext}} \leq 0.57$. The selected range causes spiral seeds to drift while maintaining an intact single-core structure. Note that in each case, two layers are coupled only when a spiral has fully evolved and occupies its lattice. Thus, in the preparation phase, the setting $D = 0$ and $\varphi_{\text{ext}} = 0$ is used. After a runtime of $t = 1500$, we set $D = 15$ and apply φ_{ext} to a single layer.

3. Results

In the present section, the bilayer structure is visualized in a three-dimensional view. Each figure contains snapshots of drifting spirals over time. In the first subplot of each figure, the zone in which the spiral seed travels is encircled by a white square. The initial and final sites of spiral rotors are connected via a straight arrow, with the pointy end defining the meandering direction. White arrows imply that the final location of the spiral seed remains within the observable region. However, yellow arrows indicate the exit of spiral seeds as they drift outwards.

(a) Co-rotating spirals with identical tip curvature

In the following subsection, the coupling of two tightly curved spirals with identical chirality is examined. In figure 2, both spirals rotate counterclockwise, with a magnetic flux of $\varphi_{\text{ext}} = 0.54$ applied to the upper layer. Figure 2*a* depicts each layer at the onset of interlayer coupling and

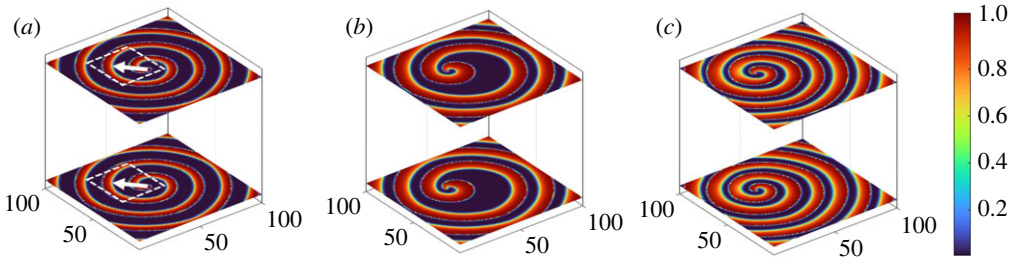

Figure 2. Coupling of co-rotating counterclockwise spirals with identical tip curvature. The of $\varphi_{ext} = 0.54$ is applied to the upper layer. The snapshots represent the temporal evolution of wave patterns in the bilayer structure, starting from $t = 0$ at (*a*) and leading to (*c*). (*a*) The onset of interlayer coupling. The final direction of drift is specified by white arrows, suggesting parallel drift to the upper left corner. (*b*) The relocated spiral seeds with amplified wavefront. (*c*) Drifted spirals stabilize spatially. Spiral rotation, meandering pattern and drift occur synchronously.

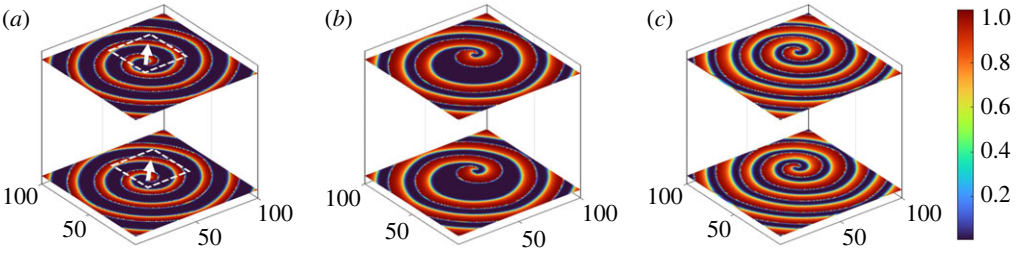

Figure 3. Coupling of co-rotating clockwise spirals with identical tip curvature. The of $\varphi_{ext} = 0.54$ is applied to the upper layer. The snapshots represent the temporal evolution of wave patterns in the bilayer structure, starting from $t = 0$ at (*a*) and leading to (*c*). Descriptions follow figure 2, but with spirals drifting toward the upper right corner of the planes, concerning the clockwise rotation.

the single-layer magnetic stimulation. Both spiral rotors drift in parallel. Owing to the interlayer connection and external forcing, wavefronts are amplified, as evidenced by the thickened red-coloured patterns in figure 2*b*. In the last snapshot of the bilayer complex, figure 2*c*, spiral seeds are spatially stable and rotate synchronously.

To identify the impact of handedness, we also investigate the coupling of two tightly curved spirals that rotate clockwise. Analogous to figure 2, in figure 3, the external forcing of $\varphi_{ext} = 0.54$ is applied to the upper layer. Figure 3*a* depicts the scenario at $t = 0$. The co-rotating spirals drift synchronously (as seen in figure 3*b*) and stabilize at corresponding locations in each lattice (figure 3*c*).

By comparing the results from figures 2 and 3, it is evident that when two identical co-rotating spirals are coupled, the meandering pattern of the reentrant seeds remains consistent. The drift direction is influenced by the chirality of the spirals and tends to align with the winding direction: if counterclockwise, spiral seeds move towards the upper left corner of the lattice, and if clockwise, the seeds shift to the upper right corner. It is noteworthy that the arrows indicating spiral drift are reflections of one another concerning the vertical symmetry line of the planes. Since the spirals have identical curvature, the same results are obtained by applying the external flux to the lower layer. The data are not shown to avoid repetition.

(b) Counter-rotating spirals with identical tip curvature

In this scenario, two tightly curved spirals of opposing chirality are coupled. Figure 4*a* illustrates the initiation of interlayer coupling and single-layer flux stimulation. The progression of

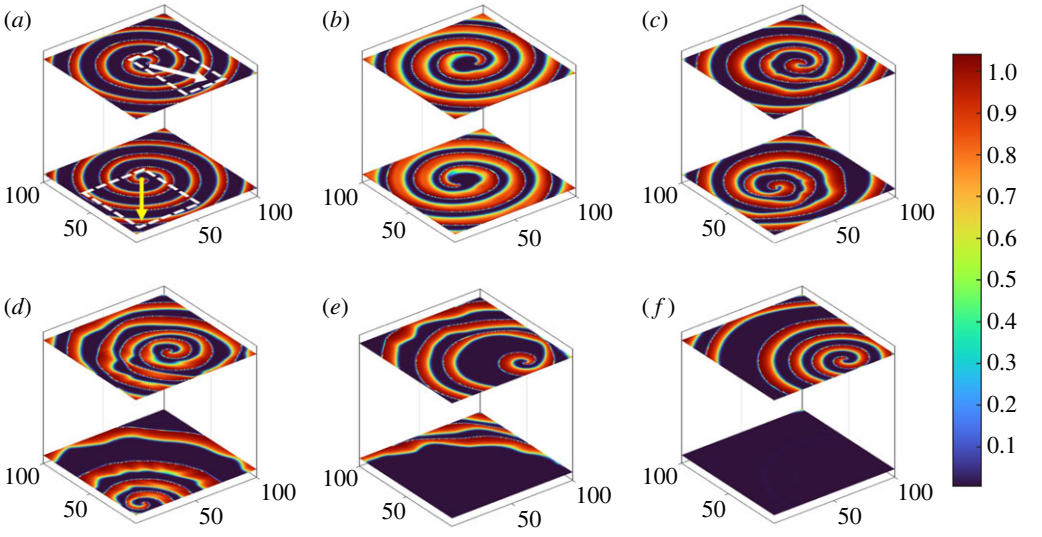

Figure 4. Coupling of counter-rotating spirals with identical tip curvature. The of $\varphi_{\text{ext}} = 0.52$ is applied to the lower layer. The temporal evolution of wave patterns in the bilayer structure is represented in sequence from $t = 0$ at (*a*) and leading to (*f*). (*a*) Patterns at the onset of interlayer coupling. The drift directions and overall regions of spiral seed movement vary between the two layers. The stimulated spiral in the lower layer exhibits greater mobility and eventually moves beyond the visible area, as marked by the yellow arrow. (*b*) Shortly after establishing the interlayer connection, the spirals intensify, and their wavefronts expand into broader circles. (*c*) The spiral seeds drift asynchronously, disrupting the wave's geometric symmetry. (*d*) The core of the lower layer's spiral travels a significant distance, nearing the plane's edge. (*e*) As the lower layer's spiral departs the plane, the upper layer's spiral seed settles into its final position. (*f*) All remaining wavefronts from the lower layer are pushed outward, allowing the upper layer's spiral to achieve symmetry and stability.

wave patterns and the rotor's translational movement can be inferred from the sequence of snapshots spanning figure 4*b–f*. An external forcing flux, $\varphi_{\text{ext}} = 0.52$, is applied to the lower layer. Supplementary details in figure 4*a* highlight the eventual locations of the spiral cores after their drift, the regions of spiral meandering, and the drift's direction. The opposing chirality of the spirals prompts the stimulated lattice to manifest a distinct drift pattern. Figure 4*b* reveals that soon after the establishment of interlayer connectivity, wavefronts in both layers intensify. This amplification stems from the combined effects of the two travelling waves and the added external stimulation. Over time, as depicted in figure 4*c*, the divergent winding directions cause the spirals to drift asynchronously in different trajectories, and the waves' geometric symmetry becomes disrupted. Consequently, the core of the spiral in the lower layer travels a more considerable distance, nearing the plane's boundaries, as shown in figure 4*d*. By figure 4*e*, the spiral in the lower layer exits the observable region, and the spiral seed in the upper layer stabilizes in its final spot. However, its wavefronts remain perturbed due to influences from the lower layer. In figure 4*f*, all residual wavefronts from the lower layer are expelled, and the wave patterns in the upper layer revert to their original symmetry, rotating about a stationary core. A few iterations after the snapshot in figure 4*f*, the same spiral wave from the upper layer re-emerges in the lower layer, owing to the temporary silence of the lower layer and the presence of interlayer flux coupling.

Comparing the results from figure 4 with those of figures 2 and 3, it's evident that the chirality of spirals influences identical spirals to drift in distinct directions. The uniformity of drift is disrupted when spirals exhibit antirotating behaviour. Given that the spirals share identical tip curvature, directing an external flux to the upper layer results in an almost reverse drift direction, concerning the lattice line of symmetry. In figure 4, the lattice with a counterclockwise spiral (in the lower layer) is subjected to force. If we apply stimulation to the upper layer with a clockwise spiral, the chirality of the stimulated spiral dictates the overall drift direction in both layers, as

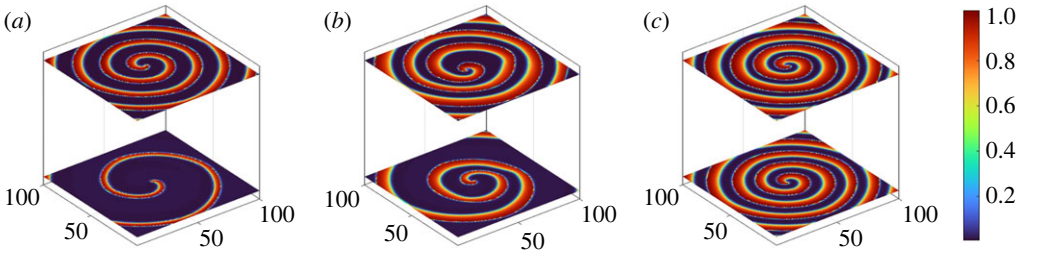

Figure 5. Coupling of co-rotating spirals with non-identical tip curvature. The $\varphi_{ext} = 0.55$ is applied to the upper layer whose spiral is tightly curved. Snapshots from (*a*) to (*d*) are chronologically arranged starting from $t = 0$. (*a*) The onset of interlayer coupling. (*b*) Both spiral wavefronts are intensified and rotate asynchronously. (*c*) Spirals gain similar patterns and rotate synchronously. The loosely curved spiral in the lower layer experiences more transformations compared to the tightly curved one in the upper layer.

deduced from figures 2 and 3. To avoid redundancy, we consider the results from figure 4 to be representative of the scenarios of coupled antirotating spirals with the same curvature.

(c) Co-rotating spirals with non-identical tip curvature

The following subsections address the coupling of non-identical spirals. The spirals depicted in figures 2–4 were characterized by tight curvature. In the upcoming results, one layer features a spiral with a gentle curve. Thus, both the amplitude of the wavefronts and the distance between consecutive travelling wavefronts differ. Metaphorically speaking, the loosely curved spiral appears to be weaker than the one with tight curvature. When interlayer coupling is activated, these loosely curved spirals intensify, aligning their geometry with that of the tightly curved spirals. Then, the unpinning and drift scenarios begin. In figures 5 and 6, the spirals in the upper layer are tightly curved, while those in the lower layer are loosely curved. In each figure, an external magnetic flux targets one of the non-identical spirals. This approach aids in determining which destabilized spiral can trigger the drift.

In figure 5, the spirals co-rotate, and the magnetic flux of $\varphi_{ext} = 0.55$ is applied to the upper layer. The onset of simulating the two non-identical spirals is captured in figure 5*a*. The combined effects of interlayer coupling and external forcing lead to an amplification of the coupled spirals' wavefronts, as illustrated in figure 5*b*. Up to this point, the rotational movements of the spiral seeds are out of sync. Over time, as the spirals adopt similar patterns, their rotations synchronize, as suggested by figure 5*c*. Notably, in this scenario, there is no significant drift. It is hypothesized that co-rotation encourages synchronization between the spirals, with the magnetic stimulation aiding the stronger spiral in amplifying the weaker one in the lower layer. It is notable that we have also explored stronger forcings, but they compromised the stability of the individual rotors, making drift analysis challenging.

In our subsequent study, the magnetic flux is applied to the lower layer, which features a travelling spiral wave with a loose curvature. The magnitude of the external flux is $\varphi_{ext} = 0.55$ as in figure 5. The sequence of events is depicted in the snapshots of figure 6. Figure 6*a* marks the start of the simulation, indicating the final drift direction and the meandering zone. Due to the external forcing destabilizing the loosely curved spiral, the difference in tip curvature between the spirals causes the stimulated lattice to display different drift patterns. Shortly after the commencement of interlayer coupling, as seen in figure 6*b*, both spirals exhibit amplified wavefronts. Notably, the loosely curved spiral strengthens, aligning its wavefront with that of the upper layer spiral. In figure 6*c*, the symmetry of the travelling wavefronts is disrupted, signalling the unpinning and onset of drift. By figure 6*d*, both spiral seeds have travelled a significant distance, approaching the plane's boundaries. However, as shown in figure 6*e*, the spiral in the lower layer drifts slightly further and exits the plane. Predictably, when a spiral seed from

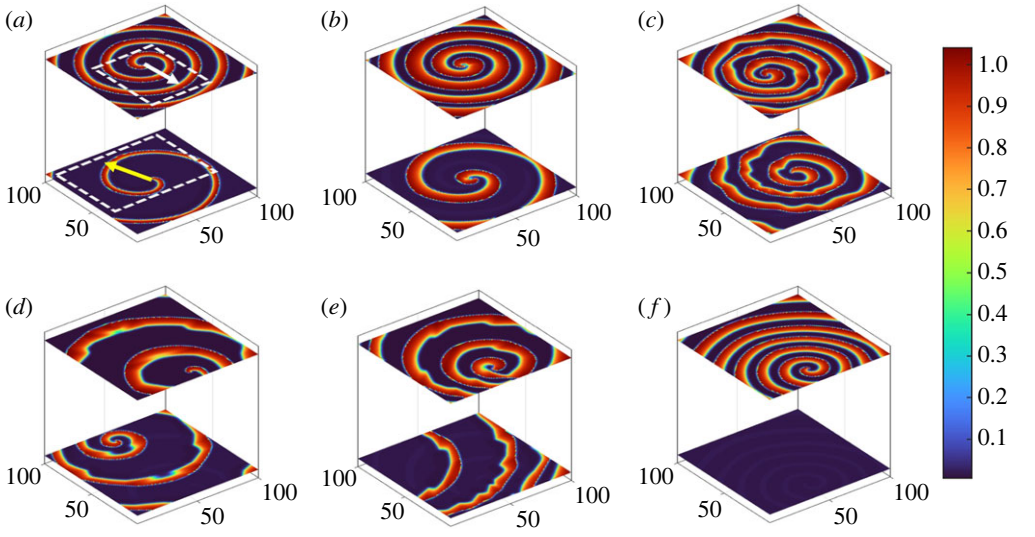

Figure 6. Coupling of co-rotating spirals with non-identical tip curvature. The $\varphi_{ext} = 0.55$ is applied to the lower layer whose spiral is loosely curved. (*a*) Patterns observed at the beginning of interlayer coupling. The spiral in the upper layer meanders within a larger area compared to the lower layer. Their drift directions are opposite. The drift distance of the seed in the lower layer is slightly greater, causing it to eventually exit the plane (as indicated by the yellow arrow). (*b*) The spirals exhibit intensified wavefronts. (*c*) Following the initial amplification, the seeds become unpinned, and the symmetry of the wavefronts is disrupted. (*d*) Both spirals approach the boundaries of the plane. (*e*) The spiral in the lower layer drifts slightly further, moving beyond the observable area, while the rotor in the upper layer becomes stationary. (*f*) With the lower layer devoid of a travelling wave, the remaining wave in the upper layer rotates, restoring its prior symmetry.

one layer departs the coupled region, the seed in the other layer achieves spatial stability. The wavefronts of the stable spiral remain disturbed until the remnants of the exited spiral are entirely outside the plane, as illustrated in figure 6*f*. Shortly after the depiction in figure 6*f*, the spiral wave from the upper layer reappears in the lower layer, due to the brief silence of the lower layer and the effect of interlayer flux coupling.

Based on the observations of co-rotating non-identical spirals in figures 5 and 6, it is evident that the loosely curved spiral tends to adopt the strength and pattern of its tightly curved counterpart, joining it in subsequent amplifications. When stimulation is directed at the tightly curved spiral, the wave evolution halts at this stage. The spiral seeds stabilize and pin to a specific spatial point, preventing any drift. However, when the loosely curved spiral is forced, the wave evolution persists, leading to unpinning and drift.

(d) Counter-rotating spirals with non-identical tip curvature

In the final scenario, two non-identical spirals rotate in opposite chirality. The external flux is once applied to the tightly curved clockwise spiral in the upper layer and, in another analysis, to the loosely curved spiral counterclockwise in the lower layer.

In figure 7, the tightly curved spiral is stimulated by $\varphi_{ext} = 0.55$. Figure 7*a* displays the initial patterns of the coupled spirals. In this case, only one spiral drifts, as indicated by the yellow arrow. As observed previously, single-layer stimulation and interlayer coupling amplify the wavefront, as shown in figure 7*b*. As the wavefronts intensify, the spiral cores become unstable and detach from their original positions. This spatial destabilization of the cores is accompanied by asymmetrically travelling wavefronts, as indicated in figure 7*c*. Contrary to previous findings, in the case of counter-rotating spirals, only the stimulated spiral drifts, while the other remains stationary, as seen in figure 7*d*. Even though the tightly-curved spiral is stimulated, which

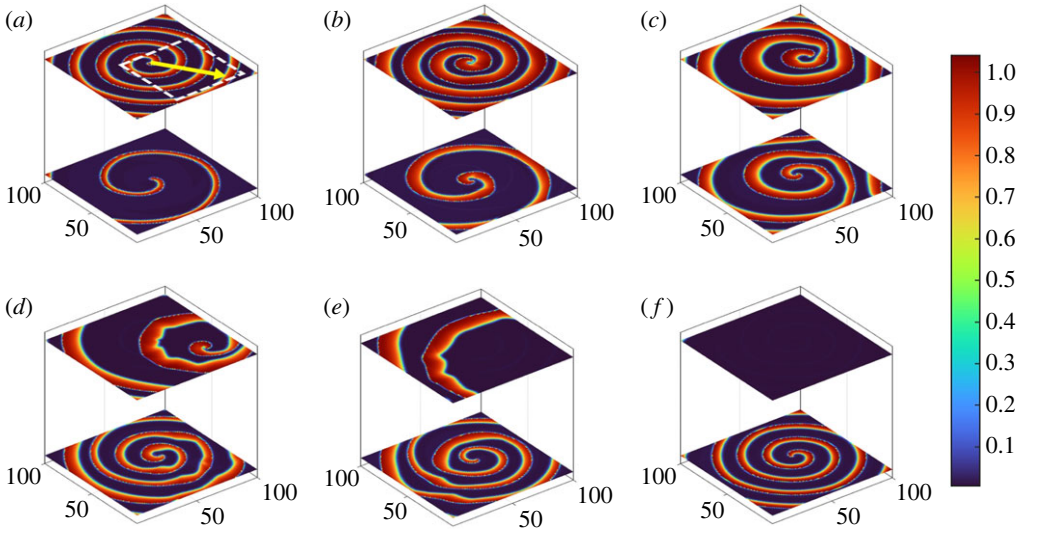

Figure 7. Coupling of counter-rotating spirals with non-identical tip curvature. The of $\varphi_{ext} = 0.55$ is applied to the upper layer whose spiral is tightly curved. (*a*) The initial patterns of coupled spirals, with one drifting as marked by a yellow arrow. (*b*) The amplification of wavefronts. (*c*) spirals become unstable, leading to spatial shifts and asymmetric wavefronts. (*d*) Only the stimulated spiral in the counter-rotating pair drifts and the other (lower layer) tends to be stationary. (*e*,*f*) The stimulated spiral exits, leaving the lower layer stable but with a stronger wavefront.

inherently strengthens the wavefronts, the same magnetic stimulation does not cause drift if the scenario is replicated in a monolayer structure. The loosely curved spiral might not drift, but its spatiotemporal activity plays a crucial role in the upper layer spiral's movement. In the subsequent image, figure 7*e*, the stimulated spiral reaches the plane boundaries and exits. Once the upper layer spiral fully exits, the lower layer achieves stability and continues to rotate from the same initial location but with a more potent wavefront, as depicted in figure 7.

The results of the loosely curved spiral stimulation are shown in figure 8. In this case, the experiments suggest that the magnetic flux of $\varphi_{ext} = 0.57$ is required for the spiral seeds to both drift and maintain stability. In the initial state of the spirals, both the seed's meandering region and their final destination are identified, as seen in figure 8*a*. In line with previous findings, the stimulated spiral drifts a greater distance and exits the plane, as marked by the yellow arrow. The concurrent amplification of wavefronts, unpinning, wavefront asymmetry and asynchronous drift of spirals over varying distances can be observed from figure 8*b–d*. By figure 8*e*, the stimulated spiral in the lower layer is eventually pushed out of the lattice, while the upper layer rotor halts near the boundary. As the lower layer remains momentarily inactive (before the reappearance of the upper layer spiral in the lower layer), the other spiral regains its original geometrical symmetry.

4. Discussion

The results indicated that, in many instances, the spiral seed drifted within a bounded zone, referred to as the 'meandering area' in this study. The meandering pattern within this area was typically circular, allowing the spiral seeds to wander freely. Regardless of whether the spirals were identical or non-identical, they began to align geometrically soon after the initiation of coupling and stimulation. This alignment was accompanied by an amplification of both spirals' wavefronts. After this stage, the spirals might become unpinned and start to drift.

In this work, destabilization emerged as the critical element leading to the drift of spiral loci. The interlayer coupling meant that destabilizing a spiral in one layer could indirectly lead to

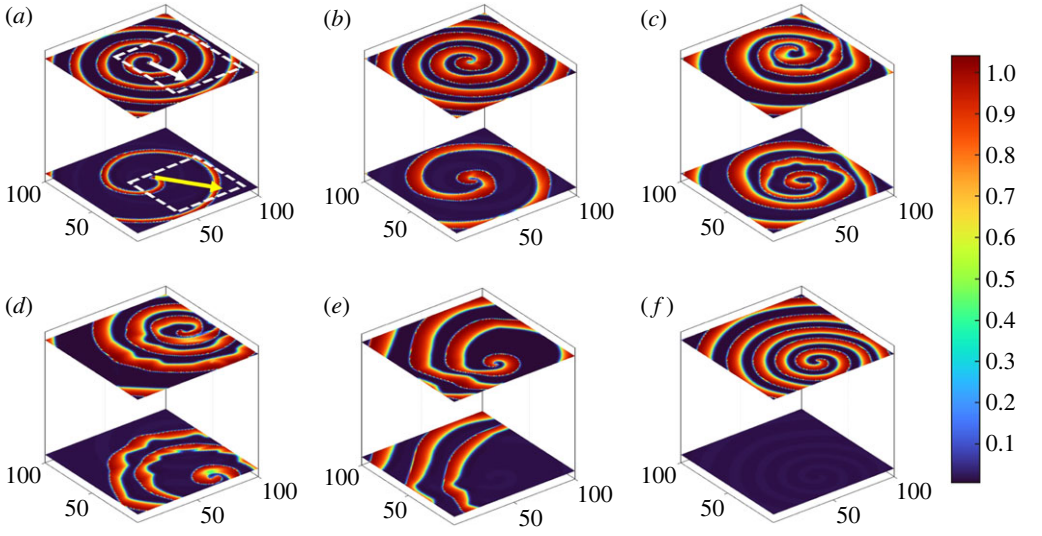

Figure 8. Coupling of counter-rotating spirals with non-identical tip curvature. The of $\varphi_{ext} = 0.57$ is applied to the lower layer whose spiral is loosely curved. (*a*) The initial patterns of coupled spirals, with both spirals drifting. (*b*) The amplification of wavefronts. (*c*) Spirals become unstable, unpin, and travel by asymmetrical wavefronts. (*d*) Both spirals drift large distances and approach the boundaries of the observable region. (*e*) The stimulated spiral drifts outward and exits, while the other spiral moves inward and stays within the lattice. (*f*) The remaining spiral becomes spatially stable and symmetrical.

the destabilization of its counterpart, heightening the likelihood of subsequent drift. Applying a proper extent of external flux to one layer could yield meandering seeds, whereas applying half such flux to both layers did not yield promising results. Simultaneously stimulating both layers with the same value of single-layer forcing could disturb the single-core spiral, forming multi-core spiral patterns. Such an occurrence was not consistent in examining spiral seed drift. Thus, the findings were derived under single-layer stimulation conditions. Under such circumstances, another necessary condition for the drift of spirals in a multi-layered structure was an appropriate coupling intensity, ensuring a strong inter-layer connection followed by a destabilizing factor.

Initially, identical spirals were analysed. The spirals' chirality then influenced the remaining drift scenario, including the direction of drifts, the meandering patterns and their synchronization. Co-rotating spirals displayed simultaneous and synchronous drift, with identical meandering trajectories and final destinations characterizing this synchronous movement. The chirality of rotation, whether clockwise or counter-clockwise, only determined the final resting place of both spiral seeds. Furthermore, this synchronized drift behaviour maintained the symmetry of the circular wavefronts across both layers. By contrast, counter-rotating identical spirals in each layer experienced asynchronous drifts in distinct directions and patterns. Such outcomes were expected when the chirality of spirals was opposite, as the propagation of wavefronts was marked by a phase difference, causing asymmetry and disturbances in the circular wavefronts. Additionally, the phase difference, coupled with opposite chirality, had the advantage of driving one spiral—precisely, the one in the directly stimulated layer—out of the lattice. For co-rotating identical spirals, the drift was not extensive enough to push the spiral cores out of the observable area. When one spiral exited the lattice, the movement of the other spiral seed ceased, becoming spatially fixed, and the symmetry of the wavefronts was reestablished. Overall, it was deduced that chirality is not a crucial factor in the drift of identical spirals.

The introduction of non-identical spirals added complexity to the drift outcomes, as differences in curvature led to variations in the amplitude and the spacing between consecutive travelling wavefronts. In these scenarios, all drifts occurred asynchronously and in unique directions.

For co-rotating spirals with differing curvatures, deciding which spiral to stimulate—either the tightly curved or the loosely curved—became critical. Stimulating the tightly curved spiral resulted in stationary spiral cores, whereas stimulating the loosely curved spiral allowed the wave progression to persist, leading to the spirals' unpinning and drift. Hence, in the case of non-identical spirals, directly destabilizing the less curved spiral was effective.

In counter-rotating non-identical spirals, stimulating the tightly curved spiral induced the drift of that particular spiral while its counterpart remained stationary. Compared to its co-rotating counterpart, this behaviour revealed the significant influence of opposing chirality on drift dynamics. Stimulating the loosely curved spiral led to the drift of both spirals, akin to the co-rotating case.

From these observations, one could infer that in the coupling of diverse rotating spirals, there is a minor chance of no drift occurring. More frequently, both spirals might drift, with the stimulated one displaying greater mobility and often moving beyond the observable area. The directions of drift and the overall meandering regions appeared complicated to decipher and didn't seem directly tied to the spirals' chirality. For instance, co-rotating spirals could drift in opposite directions, while counter-rotating seeds might journey in the same direction.

5. Conclusion

This paper offered comprehensive insights into the factors influencing the emergence of 'meandering spiral waves'. The main focus was identifying the spiral core drifts resulting from the interaction of two sustained spiral waves, each originating and existing in separate layers. The spatial analysis was expanded to a bilayer structure to achieve this, with each lattice consisting of 100×100 neurons. The nodal dynamics of each planar array were defined by the extended model of Fitzhugh Nagumo, incorporating the effects of electromagnetic induction. Spirals in each layer were connected through local chemical coupling. The spiral waves' planar movement, or drift, was indirectly influenced by this interlayer coupling, as the two layers were linearly connected via magnetic flux. Alongside the interlayer coupling, an external destabilizing factor was considered. A specific range of external magnetic flux stimulation was found to be vital for initiating drift. However, it was applied only to one layer. Simultaneously stimulating both layers with the appropriate magnitude to cause drifts disrupted the single-core spiral, forming multi-core spiral patterns. Such an occurrence was not consistent in examining spiral seed drift.

Most importantly, the unique characteristics of spiral patterns, such as chirality and tip curvature, were evaluated by various combinations of co-rotating, counter-rotating, and spirals with similar and differing, namely identical and non-identical, curvature. The setting of chemical coupling was adjusted to produce rotating spirals with loose and tight curvature. Spirals with tighter curves were characterized by higher wavefront amplitudes and closely spaced circular wavefronts travelling within the observable region. Additionally, the initial condition settings determined the spirals' chirality.

The findings indicated that an appropriate interlayer coupling intensity, combined with destabilizing a spiral in one of the layers using a specific range of external magnetic flux, can cause spirals to meander within a bounded range. When the spirals were identical in curvature, they drifted. If the spirals co-rotated, the drift occurred synchronously, and if they counter-rotated, the drifts were asynchronous, with the directly stimulated spiral leaving the observable region. The case of non-identically curved spirals introduced the complexity of deciding which spiral to stimulate. In co-rotating non-identical spirals, only stimulating the loosely curved spiral could ensure the drift of both spirals. In the case of counter-rotating spirals, at least one of the spirals, the one being directly stimulated, could drift.

Data accessibility. This article does not contain any additional data.

Declaration of AI use. We have not used AI-assisted technologies in creating this article.

Authors' contributions. D.N.H.: conceptualization, data curation, investigation, methodology, software, writing—original draft, writing—review and editing; F.P.: conceptualization, formal analysis, investigation, methodology, validation, writing—original draft, writing—review and editing; K.R.: funding acquisition,

investigation, project administration, supervision, writing—original draft, writing—review and editing; S.J.: conceptualization, funding acquisition, methodology, project administration, resources, software, supervision, writing—original draft, writing—review and editing; M.P.: funding acquisition, project administration, supervision, writing—original draft, writing—review and editing; E.K.: conceptualization, formal analysis, project administration, resources, validation, writing—original draft, writing—review and editing.

All authors gave final approval for publication and agreed to be held accountable for the work performed therein.

Conflict of interest declaration. We declare we have no competing interests.

Funding. M.P. is supported by the Slovenian Research and Innovation Agency (Javna agencija za znanstvenoraziskovalno in inovacijsko dejavnost Republike Slovenije) (grant nos. P1-0403 and N1-0232). The work is also partially funded by Centre for Nonlinear Systems, Chennai Institute of Technology, India vide funding no. CIT/CNS/2023/RP/012.

References

1. Ullner E, Zaikin A, García-Ojalvo J, Bäscones R, Kurths J. 2003 Vibrational resonance and vibrational propagation in excitable systems. *Phys. Lett. A* **312**, 348–354. (doi:10.1016/S0375-9601(03)00681-9)
2. Hempel H, Schimansky-Geier L, García-Ojalvo J. 1999 Noise-sustained pulsating patterns and global oscillations in subexcitable media. *Phys. Rev. Lett.* **82**, 3713–3716. (doi:10.1103/PhysRevLett.82.3713)
3. Ullner E, Politi A. 2016 Self-sustained irregular activity in an ensemble of neural oscillators. *Phys. Rev. X* **6**, 011015. (doi:10.1103/PhysRevX.6.011015)
4. Gomez-Marin A, Garcia-Ojalvo J, Sancho J. 2007 Self-sustained spatiotemporal oscillations induced by membrane-bulk coupling. *Phys. Rev. Lett.* **98**, 168303. (doi:10.1103/PhysRevLett.98.168303)
5. Riecke H, Madruga S. 2006 Geometric diagnostics of complex patterns: spiral defect chaos. *Chaos* **16**, 013125. (doi:10.1063/1.2171515)
6. Kundu S, Majhi S, Muruganandam P, Ghosh D. 2018 Diffusion induced spiral wave chimeras in ecological system. *Eur. Phys. J. Spec. Top.* **227**, 983–993. (doi:10.1140/epjst/e2018-800011-1)
7. Bärner U, Bär M. 2004 Pattern formation in a reaction-advection model with delay: a continuum approach to myxobacterial rippling. *Ann. Phys.* **516**, 432–441. (doi:10.1002/andp.200451607-807)
8. Schiff SJ, Huang X, Wu JY. 2007 Dynamical evolution of spatiotemporal patterns in mammalian middle cortex. *Phys. Rev. Lett.* **98**, 178102. (doi:10.1103/PhysRevLett.98.178102)
9. Davidenko JM, Pertsov AV, Salomonsz R, Baxter W, Jalife J. 1992 Stationary and drifting spiral waves of excitation in isolated cardiac muscle. *Nature* **355**, 349–351. (doi:10.1038/355349a0)
10. Samie FH, Jalife J. 2001 Mechanisms underlying ventricular tachycardia and its transition to ventricular fibrillation in the structurally normal heart. *Cardiovasc. Res.* **50**, 242–250. (doi:10.1016/S0008-6363(00)00289-3)
11. Samie FH, Mandapati R, Gray RA, Watanabe Y, Zuur C, Beaumont J, Jalife J. 2000 A mechanism of transition from ventricular fibrillation to tachycardia. *Circ. Res.* **86**, 684–691. (doi:10.1161/01.RES.86.6.684)
12. Rappel WJ, Krummen DE, Baykaner T, Zaman J, Donsky A, Swarup V, Miller JM, Narayan SM. 2022 Stochastic termination of spiral wave dynamics in cardiac tissue. *Front. Network Physiol.* **2**, 809532. (doi:10.3389/fnetp.2022.809532)
13. DeTal N, Kaboudian A, Fenton HF. 2022 Terminating spiral waves with a single designed stimulus: teleportation as the mechanism for defibrillation. *Proc. Natl Acad. Sci.* **119**, e2117568119. (doi:10.1073/pnas.2117568119)
14. Yuan G, Gao Z, Yan S, Wang G. 2021 Termination of a pinned spiral wave by the wave train with a free defect. *Nonlinear Dyn.* **104**, 2583–2597. (doi:10.1007/s11071-021-06390-7)
15. Nagy-Ungvarai Z, Ungvarai J, Müller SC. 1993 Complexity in spiral wave dynamics). *Chaos* **3**, 15–19. (doi:10.1063/1.165973)
16. Mikhailov AS, Davydov VA, Zykov VS. 1994 Complex dynamics of spiral waves and motion of curves. *Physica D* **70**, 1–39. (doi:10.1016/0167-2789(94)90054-X)

17. Panfilov AV, Keldermann RH, Nash MP. 2007 Drift and breakup of spiral waves in reaction–diffusion–mechanics systems. *Proc. Natl Acad. Sci. USA* **104**, 7922–7926. (doi:10.1073/pnas.0701895104)
18. Punacha S, Kumara AN, Shajahan TK. 2020 Theory of unpinning of spiral waves using circularly polarized electric fields in mathematical models of excitable media. *Phys. Rev. E* **102**, 032411. (doi:10.1103/PhysRevE.102.032411)
19. Pumir A, Krinsky V. 1999 Unpinning of a rotating wave in cardiac muscle by an electric field. *J. Theor. Biol.* **199**, 311–319. (doi:10.1006/jtbi.1999.0957)
20. Shajahan TK, Berg S, Luther S, Krinski V, Bittihn P. 2016 Scanning and resetting the phase of a pinned spiral wave using periodic far field pulses. *New J. Phys.* **18**, 043012. (doi:10.1088/1367-2630/18/4/043012)
21. Punacha S, Berg S, Sebastian A, Krinski VI, Luther S, Shajahan TK. 2019 Spiral wave unpinning facilitated by wave emitting sites in cardiac monolayers. *Proc. R. Soc. A* **475**, 20190420. (doi:10.1098/rspa.2019.0420)
22. Boccia E, Luther S, Parlitz U. 2017 Modelling far field pacing for terminating spiral waves pinned to ischaemic heterogeneities in cardiac tissue. *Phil. Trans. R. Soc. A* **375**, 20160289. (doi:10.1098/rsta.2016.0289)
23. Feng X, Gao X, Pan DB, Li BW, Zhang H. 2014 Unpinning of rotating spiral waves in cardiac tissues by circularly polarized electric fields. *Sci. Rep.* **4**, 4831. (doi:10.1038/srep04831)
24. Hu Y, Ding Q, Wu Y, Jia Y. 2023 Polarized electric field-induced drift of spiral waves in discontinuous cardiac media. *Chaos Solitons Fractals* **175**, 113957. (doi:10.1016/j.chaos.2023.113957)
25. Hussaini S *et al.* 2021 Drift and termination of spiral waves in optogenetically modified cardiac tissue at sub-threshold illumination. *eLife* **10**, e59954. (doi:10.7554/eLife.59954)
26. Xia YX, Zhi XP, Li TC, Pan JT, Panfilov AV, Zhang H. 2022 Spiral wave drift under optical feedback in cardiac tissue. *Phys. Rev. E* **106**, 024405. (doi:10.1103/PhysRevE.106.024405)
27. Yuan G, Liu P, Shi J, Wang G. 2023 Dynamics and control of spiral waves under feedback derived from a moving measuring point. *Chaos, Solitons Fractals* **168**, 113220. (doi:10.1016/j.chaos.2023.113220)
28. Hörning M, Isomura A, Agladze K, Yoshikawa K. 2009 Liberation of a pinned spiral wave by a single stimulus in excitable media. *Phys. Rev. E* **79**, 026218. (doi:10.1103/PhysRevE.79.026218)
29. Rappel WJ. 2022 Intermittent trapping of spiral waves in a cardiac model. *Phys. Rev. E* **105**, 014404. (doi:10.1103/PhysRevE.105.014404)
30. Li TC, Pan DB, Zhou K, Jiang R, Jiang C, Zheng B, Zhang H. 2018 Jacobian-determinant method of identifying phase singularity during reentry. *Phys. Rev. E* **98**, 062405. (doi:10.1103/PhysRevE.98.062405)
31. Li QH *et al.* 2021 Finding type and location of the source of cardiac arrhythmias from the averaged flow velocity field using the determinant-trace method. *Phys. Rev. E* **104**, 064401. (doi:10.1103/PhysRevE.104.064401)
32. He YJ *et al.* 2021 Topological charge-density method of identifying phase singularities in cardiac fibrillation. *Phys. Rev. E* **104**, 014213. (doi: 10.1103/PhysRevE.104.014213)
33. Weiler N, Wood L, Yu J, Solla SA, Shepherd GM. 2008 Top-down laminar organization of the excitatory network in motor cortex. *Nat. Neurosci.* **11**, 360–366. (doi:10.1038/nn2049)
34. Luo J, Zhang B, Zhan M. 2009 Frozen state of spiral waves in excitable media. *Chaos* **19**, 033133. (doi:10.1063/1.3224034)
35. Xie F, Weiss JN. 2007 Interaction and breakup of inwardly rotating spiral waves in an inhomogeneous oscillatory medium. *Phys. Rev. E* **75**, 016107. (doi:10.1103/PhysRevE.75.016107)
36. Winston D, Arora M, Maselko J, Gáspár V, Showalter K. 1991 Cross-membrane coupling of chemical spatiotemporal patterns. *Nature* **351**, 132–135. (doi:10.1038/351132a0)
37. Feng Y, Khalaf AJM, Alsaadi FE, Hayat T, Pham VT. 2019 Spiral wave in a two-layer neuronal network. *Eur. Phys. J. Spec. Top.* **228**, 2371–2379. (doi:10.1140/epjst/e2019-900082-6)
38. Wang Z, Rostami Z, Jafari S, Alsaadi FE, Slavinec M, Perc M. 2019 Suppression of spiral wave turbulence by means of periodic plane waves in two-layer excitable media. *Chaos, Solitons Fractals* **128**, 229–233. (doi:10.1016/j.chaos.2019.07.045)
39. Ge M, Lu L, Xu Y, Zhan X, Yang L, Jia Y. 2019 Effects of electromagnetic induction on signal propagation and synchronization in multilayer Hindmarsh-Rose neural networks. *Eur. Phys. J. Spec. Top.* **228**, 2455–2464. (doi:10.1140/epjst/e2019-900006-2)

40. Diagne K, Bury TM, Deyell MW, Laksman Z, Shrier A, Bub G, Glass L. 2023 Rhythms from two competing periodic sources embedded in an excitable medium. *Phys. Rev. Lett.* **130**, 028401. (doi:10.1103/PhysRevLett.130.028401)
41. WeiKoh JE *et al.* 2022 Application of local configuration pattern for automated detection of schizophrenia with electroencephalogram signals. *Expert Syst.* e12957. (doi:10.1111/exsy.12957)
42. Zhan M, Luo J, Gao J. 2007 Chirality effect on the global structure of spiral-domain patterns in the two-dimensional complex Ginzburg-Landau equation. *Phys. Rev. E* **75**, 016214. (doi:10.1103/PhysRevE.75.016214)
43. Comtois P, Kneller J, Nattel S. 2005 Of circles and spirals: bridging the gap between the leading circle and spiral wave concepts of cardiac reentry. *EP Europace* **7**, S10–S20. (doi:10.1016/j.eupc.2005.05.011)
44. Franović I, Perc M, Todorović K, Kostić S, Burić N. 2015 Activation process in excitable systems with multiple noise sources: large number of units. *Phys. Rev. E* **92**, 062912. (doi:10.1103/PhysRevE.92.062912)
45. Franović I, Omel'chenko OE, Wolfrum M. 2018 Phase-sensitive excitability of a limit cycle. *Chaos* **28**, 071105. (doi:10.1063/1.5045179)
46. Lindner B, Schimansky-Geier L. 1999 Analytical approach to the stochastic FitzHugh-Nagumo system and coherence resonance. *Phys. Rev. E* **60**, 7270–7276. (doi:10.1103/PhysRevE.60.7270)
47. Lindner B, Schimansky-Geier L. 2000 Coherence and stochastic resonance in a two-state system. *Phys. Rev. E* **61**, 6103–6110. (doi:10.1103/PhysRevE.61.6103)
48. Ma J, Wang Y, Wang C, Xu Y, Ren G. 2017 Mode selection in electrical activities of myocardial cell exposed to electromagnetic radiation. *Chaos Solitons Fractals* **99**, 219–225. (doi:10.1016/j.chaos.2017.04.016)
49. Majhi S, Ghosh D. 2018 Alternating chimeras in networks of ephaptically coupled bursting neurons. *Chaos* **28**, 083113. (doi:10.1063/1.5022612)
50. Ding Q, Wu Y, Hu Y, Liu C, Hu X, Jia Y. 2023a Tracing the elimination of reentry spiral waves in defibrillation: temperature effects. *Chaos Solitons Fractals* **174**, 113760. (doi:10.1016/j.chaos.2023.113760)
51. Ding Q, Wu Y, Yu D, Li T, Jia Y. 2023b Inter-layer propagation of spiral waves: effects of time-varying defect blocks and magnetic flows. *Phys. Lett. A* **489**, 129154. (doi:10.1016/j.physleta.2023.129154)
52. Wu F, Wang C, Xu Y, Ma J. 2016 Model of electrical activity in cardiac tissue under electromagnetic induction. *Sci. Rep.* **6**, 28. (doi:10.1038/s41598-016-0031-2)
53. Ma J, Mi L, Zhou P, Xu Y, Hayat T. 2017 Phase synchronization between two neurons induced by coupling of electromagnetic field. *Appl. Math. Comput.* **307**, 321–328. (doi:10.1016/j.amc.2017.03.002)
54. Roth BJ. 2001 Meandering of spiral waves in anisotropic cardiac tissue. *Physica D* **150**, 127–136. (doi:10.1016/S0167-2789(01)00145-2)
55. Dierckx H, Brisard E, Verschelde H, Panfilov AV. 2013 Drift laws for spiral waves on curved anisotropic surfaces. *Phys. Rev. E* **88**, 012908. (doi:10.1103/PhysRevE.88.012908)
56. Ding Q, Wu Y, Li T, Yu D, Jia Y. 2023 Metabolic energy consumption and information transmission of a two-compartment neuron model and its cortical network. *Chaos Solitons Fractals* **171**, 113464. (doi:10.1016/j.chaos.2023.113464)